Electromagnetic Imaging in Stratified Media by Means of a Finite-Element Variable-Exponent Inversion Approach

Valentina Schenone, Claudio Estatico, Matteo Pastorino, Andrea Randazzo, and Alessandro Fedeli

Abstract – An electromagnetic imaging technique for the characterization of targets embedded in stratified media is proposed. The method aims at reconstructing the distributions of the dielectric properties from scattering S-parameters measurements through a non-linear inversion technique in variable-exponent Lebesgue spaces merged with a finite-element formulation. The proposed method is validated in a numerically simulated three-layer scenario involving both single and multiple targets, showing good reconstruction capabilities.

1. Introduction

Electromagnetic imaging is an effective approach for performing non-invasive diagnostics in the presence of layered media, such as for subsurface prospection, soil mapping, road pavement monitoring, and non-destructive testing in industrial scenarios [1–4].

Qualitative and radar-based techniques represent commonly adopted approaches in this context [5–7]. On the one hand, they are fast and less computational demanding; on the other, they usually provide only limited information of the target. Quantitative inverse scattering techniques constitute effective alternative approaches, which have the main advantage of providing the full distributions of dielectric properties of the inspected scenario. However, they require dealing with an ill-posed and non-linear problem. Several approaches have been proposed to address this task (e.g., [8–11]).

A promising class of quantitative techniques is represented by methods formulated in variable exponent Lebesgue spaces $L^{p(\cdot)}$ [12–14], which have been found particularly efficient thanks to the possibility of adaptively tuning the exponent function that defines the space of unknowns, such as to promote sparsity in a subregion of the imaged area.

Manuscript received 26 December 2022.

Valentina Schenone, Matteo Pastorino, Andrea Randazzo, and Alessandro Fedeli are with the Department of Electrical, Electronic, Telecommunications Engineering, and Naval Architecture, University of Genoa, Via all'Opera Pia 11A, 16145 Genoa, Italy; e-mail: valentina.schenone@edu.unige.it, matteo.pastorino@unige.it, andrea.randazzo@unige.it, alessandro.fedeli@unige.it.

Claudio Estatico is with the Department of Mathematics, University of Genoa, Via Dodecaneso 35, 16146 Genova, Italy; e-mail: estatico@dima.unige.it.

In this article, an electromagnetic imaging technique for the detection of unknown targets embedded in stratified media is presented, combining a non-linear inversion formulated in variable exponent spaces $L^{p(\cdot)}$ with a finite-element (FE) solver. Such an approach extends the one initially present in [12] for stroke detection by allowing the inspection of targets embedded in a subsurface scenario where stratified media are present. Moreover, since the approach directly works on the S-parameters at antenna ports, a better modeling of the measurements setup with respect to [13–15] can be achieved. Numerical validation in the presence of a three-layer scenario with single and multiple embedded targets is presented.

2. Inversion Procedure

The detection of targets included in a multi-layer environment is considered (Figure 1). In detail, a set of N antennas, operating in a multi-static and multi-view configuration, are located along a measurement line of length l (parallel to the x-axis). The scenario is composed of three layers of non-magnetic materials: the upper one is air (characterized by the dielectric properties of vacuum), the intermediate one has height h_2 and complex relative dielectric permittivity $\varepsilon_{r,2}$, and the lower one has complex relative dielectric permittivity $\varepsilon_{r,3}$. The targets under test (assumed to be cylindrical with axis directed along the z-axis) are illuminated by a z-polarized incident radiation and are located within a rectangular $D \times W$ investigation region I in the lower layer. Under these assumptions, a two-dimensional setting is considered.

The dielectric properties of the investigation region are described in terms of the contrast function $\chi(\mathbf{r}) = \varepsilon_r(\mathbf{r})/\varepsilon_{r,3} - 1$, $\mathbf{r} \in I$. The aim of the imaging procedure is to retrieve such an unknown function from measurements of the scattering parameters collected between antenna pairs h, k, $h \neq k$. It is assumed to have at our disposal data with and without targets, that is, S_{hk}^{tot} and S_{hk}^{inc}.

The investigation domain is discretized into N triangles I_n and the z-components of incident and total electric fields when lth antenna transmits are formulated by the FE approach as $u_l^{inc,n}(\mathbf{r}) = \sum_{q=1}^{3} u_{l,q}^{inc,n} \gamma_q^n(\mathbf{r})$ and $u_l^{tot,\chi,n}(\mathbf{r}) = \sum_{q=1}^{3} u_{l,q}^{tot,\chi,n} \gamma_q^n(\mathbf{r})$ with $\mathbf{r} \in I_n$, $\gamma_q^n(\mathbf{r})$ being triangular first-order basis functions and $u_{l,q}^{inc,n}$ $u_{l,q}^{tot,\chi,n}$coefficients of expansion in basis functions [16].

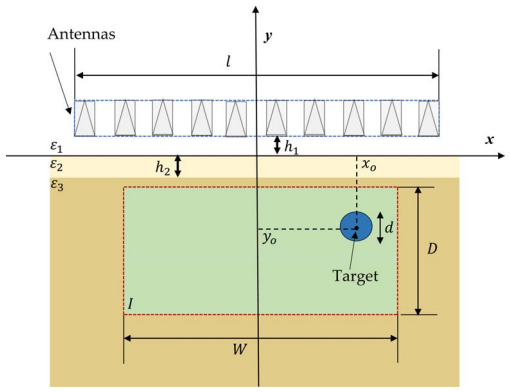

Figure 1. Configuration of the problem in stratified media.

Moreover, the unknown function is assumed constant in each triangle and represented as an array $\underline{\chi} = [\chi^1, \ldots, \chi^N]^T$.

The scattering S-parameters $S_{hk}^{SC} = S_{hk}^{tot} - S_{hk}^{inc}$ and contrast function are related as [17]

$$S_{hk}^{SC} = \alpha_{hk} \sum_{n=1}^{N} \chi^n \sum_{r=1}^{3} \sum_{s=1}^{3} u_{h,r}^{inc,n} u_{k,s}^{tot,\chi,n} T_{r,s}^n \qquad (1)$$

where $\alpha_{hk} = -j\omega\varepsilon_0\varepsilon_{r,3}/2b_h b_k$, b_l are the amplitudes of the incoming waves at port l and $T_{r,s}^n = \int_{I_n} \gamma_r^n(\mathbf{r}')\gamma_s^n(\mathbf{r}')d\mathbf{r}'$.

Considering measurements collected from all the possible pairs of transmitting and receiving antennas, the inverse problem is described by the system of equations

$$\begin{bmatrix} \Sigma_{12}(\underline{\chi}) \\ \vdots \\ \Sigma_{hk}(\underline{\chi}) \\ \vdots \\ \Sigma_{HK}(\underline{\chi}) \end{bmatrix} = \begin{bmatrix} S_{12}^{SC} \\ \vdots \\ S_{hk}^{SC} \\ \vdots \\ S_{HK}^{SC} \end{bmatrix} \qquad (2)$$

where $H = N$, $K = N - 1$, and $\Sigma_{hk}\left(\underline{\chi}\right) = \alpha_{hk} \sum_{n=1}^{N} \chi^n \sum_{r=1}^{3} \sum_{s=1}^{3} u_{h,r}^{inc,n} u_{k,s}^{tot,\chi,n} T_{r,s}^n$. It is worth remarking that the total internal field and the corresponding coefficients $u_{l,q}^{tot,\chi,n}$ in turn depend on values of the unknown contrast function in array $\underline{\chi}$, thus leading to a non-linear problem.

An inexact Newton procedure [18] formulated in the framework of $L^{p(\cdot)}$ spaces is used to invert (2). This method solves the non-linear problem by means of two iterative cycles [19]. At first, (2) is linearized around the current solution, starting with initial guess $\underline{\chi}_0 = 0$. Then the linearized problem is solved by a Landweber-like method in $L^{p(\cdot)}$ spaces [12, 19]. In each step, incident and total field coefficients $u_{l,q}^{inc,n}$, $u_{l,q}^{tot,\chi,n}$ due to the current solution are computed by using the FE method (more details can be found in [16]). Moreover, the exponent function $p(\mathbf{r})$, $\mathbf{r} \in I$, defining the adopted variable-exponent space, is adaptively updated at each outer iteration by applying a linear mapping between the normalized magnitude of the current solution $\underline{\chi}_i$ and the interval $\left[m_p, M_p\right]$ with $1 \leq m_p < M_p$ [15]. In this way, the exponent function assumes low values in the background to promote sparsity of the solution and prevent ringing effects, whereas higher values in the target region allow keeping a good reconstruction of smooth profiles as well. Such an adaptively variable exponent function $p(\mathbf{r})$ defines the exponent of space of unknowns Y, and its spatial average in I is assigned as an exponent of data space X. The procedure is halted when proper convergence criteria are satisfied [15].

3. Numerical Results

A numerical assessment of the proposed method has been performed. In particular, a set of $N = 10$ waveguide antennas with a cross section of size $a = 6$ cm (along the x-axis) and $d = 8$ cm (along the y-axis), filled with a material of relative dielectric permittivity $\varepsilon_{r,w} = 36$, has been considered. The antennas are placed along a line at height $h_1 = 3$ cm from the soil and have a distance of $h = 5.5$ cm between adjacent elements along a measurement line of length $l = 1.095$ m. The upper layer is air (characterized by $\varepsilon_{r,1} = 1$), whereas the lowest layer is characterized by $\varepsilon_{r,3} = (3 - j0.0036)$ (i.e., a dry sandy soil has been considered). The intermediate layer has thickness $h_2 = 6$ cm, and tests with different values of its relative complex permittivity have been carried out. In particular, such a layer has been characterized by values of the relative dielectric permittivity $\varepsilon_{r,2} = \varepsilon_{r,3} + \delta$, with $\delta = \{-1, 1, 5, 9\}$, that is, $Re\{\varepsilon_{r,2}\} = \{2, 4, 8, 12\}$. A void target (i.e., having relative dielectric permittivity $\varepsilon_{r,t} = 1$) with a circular cross section of diameter $d = 14$ cm is positioned at $(x_o, y_o) = (-15, -20)$ cm.

Forward simulations to obtain the total and incident scattering parameters have been performed by the FE solver at $f = 550$MHz. Then multiplicative Gaussian noise with a percentage of 3% has been added to the total S-parameters. The simulation domain has been discretized with a frontal Delaunay algorithm using the Gmsh open-source tool [20] with maximum edge length $e_I = 0.2$ cm at antenna ports and $e_I = 0.5$ cm otherwise. Absorbing boundary conditions are enforced by using a perfectly matched anisotropic absorber [16].

For the solution of the inverse problem, an investigation domain of size $W = 60$ cm and $D = 40$ cm, centered at $(x_I.y_I) = (0, -28)$ cm, discretized with maximum edge length $e_I = 0.6$ cm, has been considered. The inversion method has been run by setting maximum numbers of inexact Newton/Landweber iterations, $L = 50$; threshold on residual relative variation, $th = 0.01$; and range of the exponent function, $\left[m_p, M_p\right] = [1.3, 2.0]$.

The reconstruction method has been quantitatively evaluated through the relative error on the dielectric permittivity in the region where the target is contained (I_{tar}) and in the background (I_{bg}), defined as

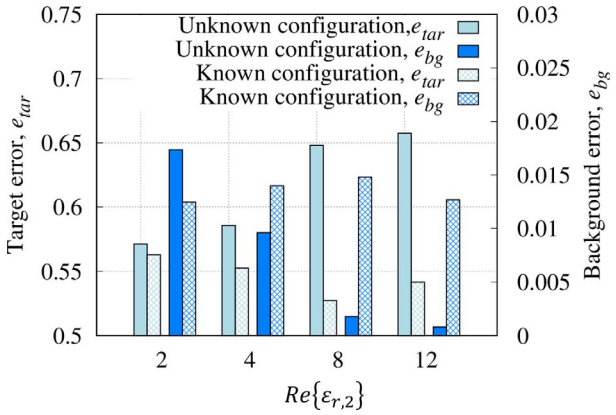

Figure 2. Relative reconstruction errors in the target and in the background region versus the real part of the relative dielectric permittivity of the intermediate soil layer, $Re\{\varepsilon_{r,2}\}$.

$$e\begin{Bmatrix} tar \\ bg \end{Bmatrix} = \frac{1}{N\begin{Bmatrix} tar \\ bg \end{Bmatrix}} \sum_{n\in\begin{Bmatrix} I_{tar} \\ I_{bg} \end{Bmatrix}} \frac{\left|\varepsilon_{r,n} - \overline{\varepsilon_{r,n}}\right|}{\left|\overline{\varepsilon_{r,n}}\right|} \tag{3}$$

where $N\begin{Bmatrix} tar \\ bg \end{Bmatrix}$ is the number of elements in the respective regions, $\varepsilon_{r,n}$ is the reconstructed relative complex dielectric permittivity in the nth element, and $\overline{\varepsilon_{r,n}}$ the corresponding reference value.

First, the inversion has been performed considering the exact configuration of the layered background, known as a priori information. Then a simplified homogeneous soil characterized by $\varepsilon_{r,3}$ (i.e., a two-layer configuration) has been assumed to analyze the effects of the uncertainty in the background knowledge.

Figure 2 reports the reconstruction errors for all the considered cases. Moreover, Figures 3 and 4 show two examples of the distributions of the reconstructed real part of the dielectric permittivity (with superimposed the actual target geometry) achieved with $Re\{\varepsilon_{r,2}\} = 4$ and $Re\{\varepsilon_{r,2}\} = 12$ when the layered structure is unknown (Figures 3a and 4a) or when it is exactly modeled in the inversion (Figures 3b and 4b). As expected, when the exact structure is unknown, the reconstruction is good (and comparable to the case of exact knowledge) when the dielectric permittivity of the intermediate layer is similar to that of the lower one (e.g., as in Figure 3a), but the performance deteriorates when dielectric properties become significantly different. In particular, for $Re\{\varepsilon_{r,2}\} \geq 12$, the target is not recovered (Figure 4a). Conversely, when the exact structure is considered in the inversion, the target is always correctly localized, its shape is recovered, and a suitable reconstruction of dielectric permittivity is achieved, as confirmed by the error values in Figure 2 and by the examples in Figures 3b and 4b.

As an additional test, the performance of the method has been validated when two targets are present in the investigation domain. In particular, an additional

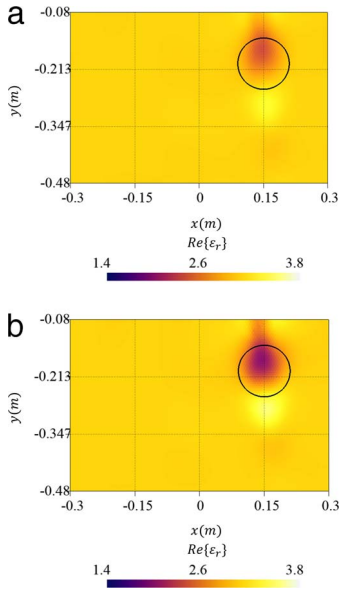

Figure 3. Reconstructed distributions of the real part of relative dielectric permittivity with $Re\{\varepsilon_{r,2}\} = 4$ and inversion with (a) unknown and (b) known layered configuration.

target of rectangular cross section with sides $l_M = 10$ cm and $l_m = 4$ cm characterized by $\varepsilon_{ro,2} = 6$ has been added at $(x_{o,2}.y_{o,2}) = (-10, 25)$ cm, and the intermediate layer is characterized by $\varepsilon_{r,2} = (4 - j0.0036)$. All the other parameters are the same of the previous cases. The reconstructed distribution of the real part of dielectric permittivity is shown in Figure 5. As can be noticed, both targets are localized, and their dielectric properties are correctly identified. Moreover, geometries are recovered quite well, although some artifacts are visible in the background. The reconstruction errors

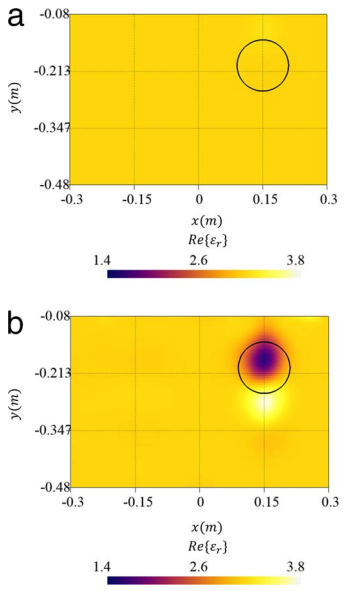

Figure 4. As in Figure 3 but with $Re\{\varepsilon_{r,2}\} = 12$.

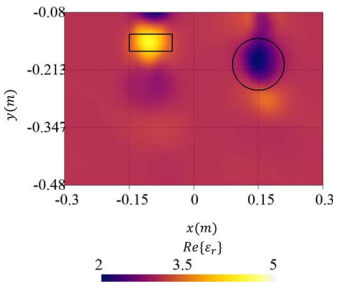

Figure 5. Reconstructed distributions of the relative dielectric permittivity in the case of two included targets.

in the background region and in the target region are $e_{bg} = 0.0276$ and $e_{tar} = 0.578$, respectively. Finally, with the aim of comparison, inversion in Hilbert space (i.e., $p = 2$) has been considered, and the reconstruction errors in the target and in the background regions are $e_{bg} = 0.0503$ and $e_{tar} = 0.619$, respectively. As can be noticed, variable-exponent Lebesgue spaces allow reconstruction errors to be smaller.

4. Conclusions

An approach to characterize targets included in stratified media is discussed in this article. An inversion procedure in variable-exponent Lebesgue spaces relying on an FE inner solver is proposed and validated in a numerically simulated environment composed of three layers. The effects of the variation of the dielectric permittivity of the intermediate layer have been analyzed. Furthermore, the behavior of the method in the presence of multiple targets of different shape has been investigated. The results show that the developed approach is potentially able to obtain a quantitative reconstruction of both the shape and the dielectric properties of targets embedded in stratified media, which is relevant in many applicable fields. Further studies will include a more extensive numerical analysis and an experimental validation of the method.

5. References

1. M. Pastorino and A. Randazzo, *Microwave Imaging Methods and Applications*, Norwood, MA, Artech House, 2018.
2. I. Catapano, A. Randazzo, E. Slob, and R. Solimene, "GPR Imaging via Qualitative and Quantitative Approaches," in A. Benedetto and L. Pajewski (eds.), *Civil Engineering Applications of Ground Penetrating Radar*, Cham, Switzerland, Springer International Publishing, 2015, pp. 239-280.
3. R. Persico, *Introduction to Ground Penetrating Radar: Inverse Scattering and Data Processing*, Hoboken, NJ, Wiley, 2014.
4. F. Soldovieri and R. Solimene, "Ground Penetrating Radar Subsurface Imaging of Buried Objects," in G. Kouemou (ed.), *Radar Technology*, London, InTech, 2010, pp. 105-126.
5. G. Ludeno, G. Gennarelli, S. Lambot, F. Soldovieri, and I. Catapano, "A Comparison of Linear Inverse Scattering Models for Contactless GPR Imaging," *IEEE Transactions on Geoscience and Remote Sensing*, **58**, 10, 2020, pp. 7305-7316.
6. L. Mertens, R. Persico, L. Matera, and S. Lambot, "Automated Detection of Reflection Hyperbolas in Complex GPR Images With No A Priori Knowledge on the Medium," *IEEE Transactions on Geoscience and Remote Sensing*, **54**, 1, January 2016, pp. 580-596.
7. A. M. Alani, M. Aboutalebi, and G. Kilic, "Applications of Ground Penetrating Radar (GPR) in Bridge Deck Monitoring and Assessment," *Journal of Applied Geophysics*, **97**, 2013, pp. 45-54.
8. M. Salucci, G. Oliveri, and A. Massa, "GPR Prospecting Through an Inverse-Scattering Frequency-Hopping Multi-focusing Approach," *IEEE Transactions on Geoscience and Remote Sensing*, **53**, 12, December 2015, pp. 6573-6592.
9. T. J. Cui, W. C. Chew, A. A. Aydiner, and S. Chen, "Inverse Scattering of Two-Dimensional Dielectric Objects Buried in a Lossy Earth Using the Distorted Born Iterative Method," *IEEE Transactions on Geoscience and Remote Sensing*, **39**, 2, February 2001, pp. 339-346.
10. J. Keskinen, A. Klotzsche, M. C. Looms, J. Moreau, J. van der Kruk, et al., "Full-Waveform Inversion of Crosshole GPR Data: Implications for Porosity Estimation in Chalk," *Journal of Applied Geophysics*, **140**, May 2017, pp. 102-116.
11. M. Hajebi and A. Hoorfar, "Multiple Buried Target Reconstruction Using a Multiscale Hybrid of Diffraction Tomography and CMA-ES Optimization," *IEEE Transactions on Geoscience and Remote Sensing*, **60**, 2022, p. 2006713.
12. A. Fedeli, V. Schenone, A. Randazzo, M. Pastorino, T. Henriksson, et al., "Nonlinear S-Parameters Inversion for Stroke Imaging," *IEEE Transactions on Microwave Theory and Techniques*, **69**, 3, March 2021, pp. 1760-1771.
13. C. Estatico, A. Fedeli, M. Pastorino, A. Randazzo, and E. Tavanti, "A Phaseless Microwave Imaging Approach Based on a Lebesgue-Space Inversion Algorithm," *IEEE Transactions on Antennas and Propagation*, **68**, 12, December 2020, pp. 8091-8103.
14. C. Estatico, A. Fedeli, M. Pastorino, and A. Randazzo, "Variable Exponent Lebesgue Space Inversion for Cross-Borehole Subsurface Imaging," *URSI Radio Science Letters*, **1**, 2019, pp. 1-5, doi: 10.46620/19-0014.
15. A. Fedeli, C. Estatico, A. Randazzo, and M. Pastorino, "Multifrequency Microwave Tomography in Lebesgue Spaces With Nonconstant Exponents," *URSI Radio Science Letters*, **2**, 2020, pp. 1-4, doi: 10.46620/20-0032.
16. G. Pelosi, R. Coccioli, and S. Selleri, *Quick Finite Elements for Electromagnetic Waves*, 2nd Ed., Norwood, MA, Artech House, 2009.
17. N. K. Nikolova, *Introduction to Microwave Imaging*. Cambridge, Cambridge University Press, 2017.
18. A. Quarteroni, R. Sacco, and F. Saleri, *Numerical Mathematics*, 2nd Ed., Berlin, Springer, 2006.
19. C. Estatico, A. Fedeli, M. Pastorino, and A. Randazzo, "Microwave Imaging by Means of Lebesgue-Space Inversion: An Overview," *Electronics*, **8**, 9, September 2019, p. 945.
20. C. Geuzaine and J.-F. Remacle, "Gmsh: A 3-D Finite Element Mesh Generator With Built-In Pre- and Post-Processing Facilities," *International Journal for Numerical Methods in Engineering*, **79**, 11, 2009, pp. 1309-1331.